Author's Accepted Manuscript

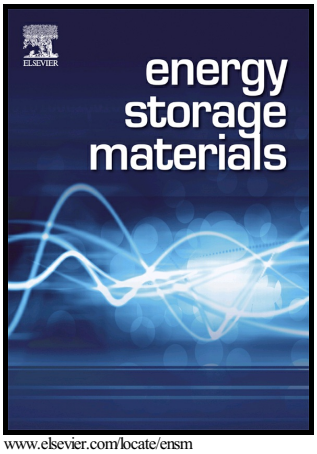

www.elsevier.com/locate/ensm

Controlling the sustainability and shape change of the zinc anode in rechargeable aqueous $Zn/LiMn_2O_4$ battery

Wenlong Xiong, Dongjie Yang, Tuan K.A. Hoang, Moin Ahmed, Jian Zhi, Xueqing Qiu, P. Chen

PII: S2405-8297(18)30047-3
DOI: https://doi.org/10.1016/j.ensm.2018.03.023
Reference: ENSM350

To appear in: *Energy Storage Materials*

Received date: 15 January 2018
Revised date: 26 March 2018
Accepted date: 30 March 2018

Cite this article as: Wenlong Xiong, Dongjie Yang, Tuan K.A. Hoang, Moin Ahmed, Jian Zhi, Xueqing Qiu and P. Chen, Controlling the sustainability and shape change of the zinc anode in rechargeable aqueous $Zn/LiMn_2O_4$ battery, *Energy Storage Materials,* https://doi.org/10.1016/j.ensm.2018.03.023

Controlling the sustainability and shape change of the zinc anode in rechargeable aqueous Zn/$LiMn_2O_4$ battery

Wenlong Xiong[a,b,c], Dongjie Yang[a,c], Tuan K. A. Hoang[b], Moin Ahmed[b], Jian Zhi[b], Xueqing Qiu[a,c,*], P. Chen[b,*]

[a] School of Chemistry and Chemical Engineering, South China University of Technology, Guangzhou 510640, China.

[b] Department of Chemical Engineering and Waterloo Institute of Nanotechnology, University of Waterloo, 200 University Avenue West, Waterloo, Ontario N2L3G1, Canada.

[c] Guangdong Engineering Research Center for Green Fine Chemicals, Guangzhou, 510641, China

p4chen@uwaterloo.ca

xueqingqiu66@163.com

[*]**Corresponding Author:** P. Chen Tel.: +1-519-888-4567 ext. 35586; fax: +1-519-888-4347. Xueqing Qiu Tel.: +86-20-8711-4722; fax: +86-20-8711-4721.

Abstract

The use of thixotropic gel electrolytes in the rechargeable hybrid aqueous battery improves the battery performance but it is required to have a corrosion inhibitor in the gel electrolyte. These inhibitors are not always friendly to the environment. In this work, we use lignin - a renewable material - to neutralize strong acid sites of the fumed silica gelling agent prior to gel preparation. Linear polarization, chronoamperometry, and ex-situ scanning electron microscopy examinations show that the new gel electrolyte reduces the corrosion on zinc (up to 43%) and supports planar zinc deposit. In other words, the shape of the zinc surface is controlled and it is further confirmed by the XRD and SEM of post-battery run anodes. Moreover, the battery using this new lignin coated fumed silica based gel electrolyte exhibits a float charge current as low as 0.0025 mA after 24 hours of monitoring, which is 30.6% lower than the reference. The capacity retention of gelled battery is as high as 82% after 1000 cycles at 4 C, which is 14% higher than the reference battery using reference liquid electrolyte under the same CC-CV test, complemented by lower self-discharge and higher rate capability. The results lead the team nearer to a commercializable gelled battery system.

Graphical Abstract

The green and sustainable QAL/FS based gel electrolyte can suppress the growth of

zinc dendrite during cycling and improve the cyclability of the rechargeable hybrid aqueous Zn/$LiMn_2O_4$ battery compared with that of the reference liquid electrolyte.

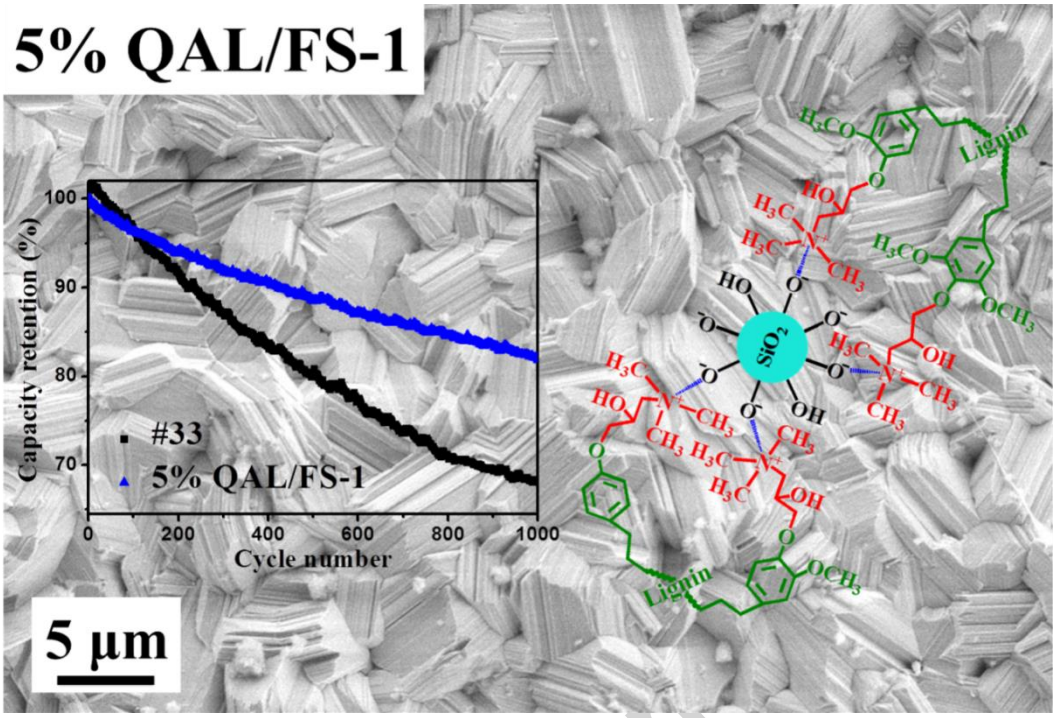

Keywords: Lignin/silica composite; corrosion; gel electrolyte; aqueous battery.

1. Introduction

Highly safe, low-cost, and environmentally friendly large-scale energy storage systems (LSESSs) are favoured to complement the efficient implementation of green and sustainable energy resources (e.g., solar, wind, and biomass energy) in the future [1–4]. To this regard, aqueous batteries have been recommended as promising approaches thanks to their low cost and eco-friendly [1–4]. Commercially available aqueous rechargeable batteries (e.g., lead–acid, nickel–cadmium, and nickel–metal hydride) cause heavy metal pollution due to corrosion and leakage [3]. They also

suffer from low energy density and limited cycle life [5]. Recently, aqueous rechargeable lithium and sodium ion batteries are attractive as they can be developed to be the most promising alternatives for state-of-the-art LSESSs because such novel batteries can address environmental sustainability and safety issues while exhibiting satisfactory cycling and rate capability [1,3–5].

In particular, a novel aqueous lithium energy storage system, namely the rechargeable hybrid aqueous battery (ReHAB), reported by P. Chen's group in 2012, can operate at a long cycle life without bringing serious environment issues [6]. The ReHAB employs commercial $LiMn_2O_4$ as the active material for the cathode, zinc foil as the anode, and an aqueous solution containing Li^+ and Zn^{2+} as the electrolyte. In order to enhance the safety of battery, the aqueous electrolyte should be developed to gel state or solid state [7–9]. Indeed, solid electrolytes have their own unique properties (e.g. high safety and good mechanical properties). But gel electrolytes, a combination of liquid and gelling agents, can reach a balance of making the most of the merits of the individual components [7]. In particular, thixotropic gel electrolytes inherit the high ionic conductivity of the aqueous electrolyte while adopting the safety advances of the solid state electrolytes. Thus, the batteries can function at high charge/discharge rates while maintenance requirements can be reduced to minimum. Hence, the research on the gel electrolytes for the ReHAB is of great significance. Moreover, the thixotropic gelling philosophy is certainly applicable in other types of batteries (e.g. valve regulated lead-acid battery), too [7,10,11].

A simple fumed silica (FS) based aqueous gel electrolyte has been successfully

implemented in the ReHAB [12]. Except for its outstanding ability to retain the water component of the electrolyte from evaporation or leaking, it can improve several performance criteria of the ReHAB, including rate capability, cyclability, self-discharge, and the suppression of dendrite growth. However, the FS-containing gel electrolyte increases the corrosion on the zinc anode [13,14] because FS is essentially regarded as a solid acid due to the existence of ionized silanol groups ($Si–O^-$) on its surface [15,16]. Both inorganic and organic chemicals, for example, $PbSO_4$ [13] and pyrazole [14], are introduced into the FS based gel electrolyte to inhibit the corrosion, respectively. Unfortunately, these chemicals are not considered green or sustainable. The method of using corrosion inhibitors does not remove corrosion fundamentally since the main cause of corrosion still exists in the electrolyte. We hypothesize that corrosion might be reduced permanently only when acid sites on the silica surface are neutralized. In this work, we attempt to solve this problem by using alkali lignin - a low cost and renewable resource [17–23]. The acidic groups ($Si–O^-$) on the surface of silica could be negated via an acid-base reaction when silica is coated with this kind of lignin [24–27].

In this work, the lignin/fumed silica composite (QAL/FS) is synthesized by a simple acid precipitation method using cationic alkali lignin and FS as raw materials, and used to prepare the QAL/FS gel electrolyte for the ReHAB. Compared to the reference liquid electrolyte, the advantages of FS gel electrolyte are maintained and even further enhanced when the new QAL/FS gel electrolyte is used, including the maintenance of open circuit voltage (OCV) performance, and the further

enhancements on suppression of dendrite growth, float charge performance, rate capability, and cycling performance. In particular, the disadvantage of the FS gel electrolyte, namely the increasing the corrosion on zinc, is fundamentally fixed when using the QAL/FS gel electrolytes.

2. Experimental section

2.1 Materials

The source and pre-treatment of pine alkali lignin (AL) were presented in our previous work [26]. $LiMn_2O_4$ was purchased from Shanshan Energy (Changsha, China). Fumed silica (FS) with particle size of 7 nm and surface area of 395 ± 25 $m^2 \cdot g^{-1}$ and lithium sulfate monohydrate ($Li_2SO_4 \cdot H_2O$, 98%) were purchased from Sigma Aldrich. Zinc sulfate heptahydrate ($ZnSO_4 \cdot 7H_2O$) was purchased from (98%) Alfa Aesar. Zinc foil (99.6% purity) was purchased from Rotometals. Other reagents, such as 60 wt% 3-chloro-2-hydroxypropyltrimethylammonium chloride (CHPTMAC) aqueous solution, lithium hydroxide (LiOH), and sodium hydroxide (NaOH), were of analytical grade and purchased from Sigma Aldrich. Sulfuric acid (H_2SO_4, 95−98 wt%, ACS plus grade) was purchased from Fisher Scientific.

2.2 Preparation of Lignin/fumed silica composite (QAL/FS)

10 g FS was dispersed in deionized water by ultrasound. Then the pH value of the obtained dispersion system was adjusted to 11.0 by using NaOH. Subsequently the QAL, which was synthesized following the same processes presented in our previous work [27], was added into the FS dispersion system, and the obtained mixture was

stirred for 30 min. The pH value of the mixture was adjusted to 4.0 by using 20 wt% H_2SO_4, and the mixture was stirred for another 30 min. The filter cake of QAL/FS was collected by vacuum filtration, during which the deionized water was used to wash the filter cake. The washed filter cake was stored and used to prepare the QAL/FS gel electrolyte. Three filter cakes of QAL/FS-1, QAL/FS-2, and QAL/FS-3 were obtained following the present process. The difference of QAL/FS-1, QAL/FS-2, and QAL/FS-3 was that the initial mass ratio of QAL to FS was 0.05:1, 0.1:1, and 0.15:1, respectively.

2.3 Preparation of batteries

Preparation of the cathode for the coin cell: 1.72 g of $LiMn_2O_4$ was mixed with 0.14 g of KS-6 graphite (Imerys Graphite & Carbon), the obtained mixture was added in 2.80 g 5 wt% solution of polyvinylidene fluoride (HSV 900, Kynar® Alchema) in N-methyl-2-pyrrolidone (Sigma Aldrich). The system was mixed by a Planetary Centrifugal Mixer (AR-100, ThinkUSA) for 10 min. Then the cathode film was obtained by coating the cathode slurry on a conductive polyethylene (PE) film (All-Spec 854-36150) and placed in 60 °C vacuum oven for 6 h. Finally the cathode was prepared by cutting from cathode film to round shape disc with diameter of 12 mm.

Preparation of the cathode for the large battery: The preparation of cathode slurry was the same as that of the cathode for the coin cell. Then the cathode film was obtained by coating the cathode slurry on a conductive graphite foil (Alfa Aesar,

99.8%) and placed in 60 °C vacuum oven for 6 h. Finally the cathode was prepared by cutting from cathode film to a piece of square film with side length of 25 mm.

Preparation of the anode: The zinc anode was prepared by polishing the commercial zinc foil using 0.3 μm polishing powder (Boehler) dispersed in deionized water and a nanocloth (Boehler). Each side of the zinc foil was polished for 10 min. The polished zinc foil was washed with deionized water, followed by rinsing with ethanol and dried at 60 °C under vacuum for 30 min. Zinc anode was obtained by cutting from the polished zinc foil to round shape disc with diameter of 12 mm for the coin cells and to a piece of square foil with side length of 40 mm for the large battery.

Preparation of the electrolyte: The aqueous electrolyte (#33) was prepared by dissolving 1 M zinc sulfate heptahydrate (Alfa Aesar Co., 98%) and 2 M lithium sulfate (Sigma Aldrich Co., 98%) in deionized water. The pH of the solution was adjusted to 4.00 ± 0.05 using sulfuric acid or lithium hydroxide solution. The FS gel electrolyte (5% FS) was prepared by mixing 5 g FS into 95 g #33 using magnetic stirring for 12 h. It should be note that the pH value of the prepared 5% FS needed to be adjusted back to 4.00 ± 0.05 using lithium hydroxide solution. The QAL/FS-1 gel electrolyte (5% QAL/FS-1) was prepared by mixing the filter cake containing 5 g QAL/FS-1 into #33 after removing a certain amount of water by evaporation. The amount of removed water of #33 should be the same as that of the filter cake of QAL/FS-1 carried. The pH value of the prepared 5% QAL/FS-1 also needed to be adjusted back to 4.00 ± 0.05 using sulfuric acid or lithium hydroxide solution. The other two gel electrolytes, QAL/FS-2 gel electrolyte (5% QAL/FS-2) and QAL/FS-3

gel electrolyte (5% QAL/FS-3), were prepared following the same process of 5% QAL/FS-1.

The battery was prepared by assembling the cathode, AGM (Absorbed Glass Mat, NSG Co.) separator wet with electrolyte, and zinc anode into a coin cell (CR 2025) and a large battery, the exterior of which is shown in Fig. S1 (Supporting information), respectively.

2.4 Electrochemical measurements

For the conductivity, corrosion, and chronoamperometry (CA) tests, the procedures were the same as that of presented in the published papers [12,13,14]. After CA test, the Zn electrodes are rinsed thoroughly by deionized water, vacuum dried and then characterized by a field emission scanning electron microscopy (SEM) (Ultra, Zeiss Corp., Germany) at 5 kV.

The float charge performance, which was presented by the float charge current and capacity, was tested by an NEWARE battery tester (NEWARE Battery Test System, Neware Co. Ltd., China) at room temperature. The test program was charging the battery from 1.4 to 2.1 V (vs. Zn^{2+}/Zn) by a constant current (CC) mode at 0.2 C rate (1 C is defined as 115 $mAh \cdot g^{-1}$), then charging the battery to maintain it at 2.1 V by a constant voltage (CV) mode for 24 h, and finally discharging the battery to 1.4 V by the CC mode at 0.2 C rate.

The open circuit voltage (OCV) was measured following the test of float charge performance. The test program was charging the battery to 2.1 V by the CC mode at

0.2 C, and then maintaining it for 24 h without charging and discharging, and finally discharging the battery to 1.4 V by the CC mode at 0.2 C rate.

The rate performance of the battery was tested by the NEWARE battery tester at various constant current (CC) charge−discharge rates from 0.2 C to 4 C at room temperature.

The galvanostatic charge−discharge cycling of the coin cells and large batteries were carried out between 1.4 and 2.1 V, in constant current−constant voltage (CC−CV) mode at room temperature at 4 C rate with the NEWARE battery tester. The current cut-off during CV charging was set at 10% of the charging current in the CC charging step at 4 C rate. After the cycling test of large batteries, the cathodes and Zn anodes are rinsed thoroughly by deionized water, vacuum dried and then characterized by a D8 Discover Powder X-ray diffractometer (XRD, Brüker Co., CuKα 1.5406 Å, 40 kV, and 30A) and a field emission scanning electron microscopy (SEM) (Ultra, Zeiss Corp., Germany) at 10 kV.

Cyclic voltammetry (CV) tests were conducted on a multichannel potentiostat (VMP3, Biologic) between 1.4 and 2.1 V at a scan rate of 0.1 $mV \cdot s^{-1}$. In addition, AC impedance measurements were performed with amplitude of 10 mV at the applied frequency range from 0.1 Hz to 1 MHz after the batteries were cycled for 10 cycles at 1 C rate. This AC impedance acquisition was conducted on a three-electrode-cell, with the battery cathode (cast on graphite foil) as the working electrode, a Pt wire as the counter electrode, and a standard calomel electrode as the reference. The impedance data were collected after the cathode was charged-discharged for 10 cycles.

The obtained data were fitted by ZView, and the Ohmic resistance, charge transferred resistance, and the Li^+ diffusion coefficient are calculated.

3. Results and Discussion

3.1 Electrochemical behaviour of electrolytes

In this part, we discuss the conductivity, corrosion, and chronamperometry (CA)of the synthetic electrolytes. Scheme 1 shows the representative structure of FS, QAL, and the prepared QAL/FS composite. The FS cannot be uniformly coated by the AL via acid precipitation due to the weak interaction between FS and AL, which is caused by the electronegativity of FS and AL in the pH range of 4 to 11. Thus, the cationic quaternary ammonium groups are grafted to AL molecules to enhance the interaction between FS and AL by providing strong electrostatic force. Because some of the acidic groups ($Si–O^–$) on the surface of FS are masked by QAL, the acidity of FS should be weakened so that its abilities to inhibit the corrosion and suppress the dendrite growth on zinc are improved. The evidences are presented in the following corrosion and CA tests.

The conductivity of the reference (#33) and the 5% FS gelled electrolyte have been reported earlier at 63.16 ± 1.30 mS cm^{-1} and 60.1 ± 0.10 mS cm^{-1} [12]. The 5% QAL/FS-1 and 5% QAL/FS-2 gel electrolytes exhibit 57.75 ± 0.36 and 54.18 ± 0.26 mS cm^{-1}. All of these gel electrolytes exhibit high conductivity, but these data are slightly lower that of the aqueous electrolyte. This is because FS and QAL are insulating materials. The increase of QAL content leads to a slight decrease of the conductivity. However, these values a still higher than those of FS-based composite

polymer electrolytes by two-order of magnitude [28,29].

The corrosion performance of different electrolytes on zinc are presented in Fig. 1. Meanwhile, corrosion potentials and current densities are displayed in Table S1 (Supporting information). In fact, the standard potential of Zn^{2+}/Zn vs. calomel reference electrode (SCE) is about −1.003 V [13,14]. The potentials of Zn^{2+}/Zn when in contact with the different electrolytes are all lower than −1.003 V. In the slightly acidic aqueous solution, the reaction of the Zn corrosion is a possible reaction because it is thermodynamically possible. Corrosion has effect on the self-discharge and the cycle life of the batteries. However, the corrosion rate can be mitigated by introducing corrosion inhibitor into the electrolyte [13,14] or modifying the surface of zinc anode [30]. In this work, a novel method, modifying the surface of FS with QAL, is applied for the first time. According to Fig. 1 and Table S1, the 5% FS shows lower corrosion potential and higher corrosion current density than that of the #33, which means FS will increase the corrosion of electrolyte on the zinc electrode. This may be due to the acid groups (Si–O^-) on the surface of FS. After the FS is coated with 5 wt% QAL, the corrosion will be slightly inhibited compared to that of the 5% FS. Unfortunately, it is still worse than the corrosion effect of the reference (#33) electrolyte, as evidenced by the lower corrosion potential and higher corrosion current density of the 5% QAL/FS-1 compared with that of the #33. When the FS is coated with 10 wt% QAL, the corrosion potential of the 5% QAL/FS-2 is increased and the corrosion current density of the 5% QAL/FS-2 is decreased to a new value which is higher and lower than that of the reference #33. This suggests that the defect in corrosion of the 5% FS

gel electrolyte compared with that of the #33 is fixed after the FS is coated with 10 wt% QAL. However, if the coating amount of QAL on FS increases to 15 wt%, the corrosion of 5% QAL/FS-3 on zinc increases compared to that of 5% QAL/FS-2. The corrosion of 5% QAL/FS-3 even becomes worse than that of the #33. This indicates that too much QAL will simultaneously exert side effect on the corrosion due to the enrichment of organic hydroxyl groups, which are available in QAL molecules (Scheme 1). When the concentration of these organic hydroxyl groups is high enough, it would introduce further acidity into the electrolyte and exert negative effect to the corrosion performance.

The CA results of Zn upon contact with different electrolytes are shown in Fig. 2a. The CA method has been employed to study the deposition of Zn^{2+} onto zinc anode and the electrolytes in other types of zinc batteries when an overpotential is applied [31]. The choice of overpotential (–120 mV) is on the basis that this potential is in the same magnitude of the polarization observed in batteries and in the dendrite formation voltage range [32,33]. When the Zn is contact with the #33, the current quickly decreases to approximately –8.5 $mA \cdot cm^{-2}$, suggesting fast nucleation on the Zn surface, and it slowly approaches –12.7 $mA \cdot cm^{-2}$ after 1 h monitoring. When the Zn is contact with the 5% FS, the current quickly decreases to approximately –10.9 $mA \cdot cm^{-2}$, which is more negative than that of the #33. This is because the increase of electronegativity on the Zn surface, which caused by the coating of negative FS, inevitably leads to more Zn^{2+} being involved in the deposition reaction on Zn surface at the beginning. However, the deposition current of Zn upon contact with the 5% FS

gradually increases and approaches –3.8 mA·cm^{-2} after 1 h monitoring. The lower the absolute value of the deposition current tending to be stable is, the lower the growth rate of Zn dendrite is [13,14]. Hence, the 5% FS shows excellent ability to suppress the growth of Zn dendrite compared to the #33. After the FS is coated with different amount of QAL, the rate of nucleation on the Zn surface at the beginning decreases, as evidenced by the lower absolute value of the deposition current, which are –7.4, –7.7, and –6.7 mA·cm^{-2}. This is because some of the electronegativity on the surface of FS is shielded by QAL. For the 5% QAL/FS-1 and 5% QAL/FS-2, the deposition current tending to be stable after 1 h monitoring are –3.3 and –3.2 mA·cm^{-2}, respectively. The absolute value of them are lower than that of the 5% FS, which indicates the advantage of dendrite suppression is improved after the FS is coated with 5 wt% or 10 wt% QAL. FS has been proven to be effective in suppressing the dendrite formation [12], but the results in this study suggest that the surface of FS should be optimized to maximize its ability to supress the dendrite growth. However, it's probably more than the optimal quantity when the coating amount of QAL on FS increases to 15 wt%. Therefore, the absolute value of the deposition current tending to be stable is 4.3 mA·cm^{-2}, which is higher than that of the 5% FS. This may be because QAL is noneffective in suppressing the dendrite formation so that too much QAL leads to the surface of FS deviating from its optimum state, which indicates that too much QAL will slightly weaken the ability of FS to suppress the growth of Zn dendrite. Hence, the 5% QAL/FS-1 and 5% QAL/FS-2 are used to evaluate the other performances of the ReHAB, according to the analyses of corrosion and CA.

The SEM images of Zn electrodes after CA test are presented in Fig. 2b. The commercial pure zinc has a nearly flat surface, with holes on the surface. This kind of surface might be resulted from the commercial production process of zinc sheets. The existence of holes is a disadvantage for aqueous batteries since the hydrogen gas (generated from zinc corrosion) would be entrapped within these holes to reduce the interface between the anode and the electrolyte. The deposition of Zn from the reference (#33) electrolyte (containing 2 M Li_2SO_4 and 1 M $ZnSO_4$, pH = 4.00) under –120 mV overpotential is dendritic. An image with larger area may be found in our previous work [14]. The deposits are rod-like with diameters in micrometer range. This kind of deposit is typical dendritic zinc which will affect the mechanical stability of the separator, change the nature of the anode–electrolyte interface, and create more porous space in the anode surface vicinity. These void spaces between the dendrites are home for the hydrogen gas generated from corrosion.

The zinc deposits from gelled electrolytes are irregular layer-like structure. All deposits from gelled electrolytes do not leave hole or gap between structures. This textural property doesn't support dendritic growth, as proved from our previous work and literature [13,30]. However, there are differences among them. The size of the layer-like features seems to increase versus the increase of lignin concentration but they don't change to other kinds of morphology. It's worth noted that, from Diggle *et al*., the dendrite is least likely to be formed on a flat and layer like surface [33].

3.2 Float charge current, open circuit voltage (OCV) and rate performance

The float charge current and float charge capacity of all batteries is presented in Fig. 3a and Table S2 (Supporting Information), respectively. This method has been used extensively in the published papers to evaluate batteries functioning at nearly full state-of-charge [12–14,34–37]. These data are extremely useful for engineers to design start-stop batteries for automobiles, uninterruptible power supplies, and for large batteries interfacing with the grid since these batteries are often working near full state of charge. The illustration in is the partial magnification of Fig. 3a. Quickly after the test started, the charging currents dropped quickly and subsequently stabilized after a few hours. Lower and stable float charge current is associated with the better float charge performance of batteries because these batteries would require less energy to compensate for self-discharge or energy runaway. After monitoring for 24 h at constant voltage of 2.1 V (by CV charging), the float charge current of coin battery using the 5% FS is about 0.0023 mA, which is lower than the 0.0036 mA of the battery using #33 and accounts for a huge decrease of 36.1%. This suggests that the 5% FS electrolyte significantly increases the float charge performance of battery compared to the reference #33 electrolyte. The float charge current of battery using the 5% QAL/FS-1 is almost the same as that of the battery using the 5% FS, and the float charge current of battery using the 5% QAL/FS-2 is approximately 0.0017 mA, which is even lower than the 0.0023 mA of battery using the 5% FS. This accounts for a tremendous decrease of 52.8% and indicates that if the surface of FS is modified by an appropriate amount of QAL to slightly decrease the electronegativity of FS, the advantage of FS in improving the float charge performance of battery is further

enhanced. The float charge capacity is positively related to the float charge current so that both of them can be used to evaluate the float charge performance of battery. Hence, the same trend is observed for the float charge capacity, as evidenced by the data shown in Table S2 (Supporting Information).

Fig. S4 (Supporting information) shows the OCV versus time of the fully charged coin batteries containing #33, FS based, and QAL/FS based electrolytes. Higher OCV value means less self-battery-discharge [12–14]. OCV value of 2000.5 mV is observed for the battery using 5% FS after 24 h monitoring. This is higher than that of the battery using #33 at 1994.0 mV, which means the storage property of battery using 5% FS is better. After the FS is coated with QAL, the advantage of FS in improving the OCV is slightly weakened, as evidenced by the slightly lower OCV value of 5% QAL/FS-1 at 1998.1 mV and 5% QAL/FS-2 at 1998.6 mV. The 5% QAL/FS-1 and 5% QAL/FS-2 retain the advantage in improving the OCV, because the OCV values of them are still higher than that of the battery using the reference #33 electrolyte.

The rate capabilities of the batteries from 0.2 C to 4 C are shown in Fig. 3b. The discharge capacities reduce upon increase of the C-rate, due to the diffusion-controlled kinetics of the lithium ion extraction/intercalation reactions [38]. The discharge capacity at 0.2 C and 0.5 C of the battery using 5% FS are almost the same as that of the battery using #33. The discharge capacity at 1 C, 2 C and 4 C of the battery using 5% FS are approximately 115.6, 106.6, and 94.1 $mAh \cdot g^{-1}$, which are higher than that of the battery using #33 at the same rate. This suggests that the rate performance of battery using the 5% FS is superior to that of battery using the #33.

For the batteries using 5% QAL/FS-1 and 5% QAL/FS-2 respectively, the discharge capacities at 0.2 C, 0.5 C and 1 C are nearly the same as that of the battery using 5% FS. Meanwhile, the discharge capacities at 2 C and 4 C are about 108.9 and 97.6 $mAh \cdot g^{-1}$, 107.2 and 95.7 $mAh \cdot g^{-1}$, respectively. The values of these discharge capacities are higher than that of #33 and 5% FS. This indicates that the advantage of FS in improving the rate performance at high rates is further enhanced after the FS is modified by QAL. Specifically, the battery using 5% QAL/FS-1 presents the best rate performance, which means the better appropriate coating amount of QAL on FS for improving the rate performance of battery is 5 wt%.

3.3 Cycling performance

Fig. 4a represents the cyclability results of battery using different electrolytes at 4 C for up to 1000 cycles. Fig. 4b represents the capacity retention results of batteries at 4 C for up to 1000 cycles. It is important to show these results together, because if the discharge capacities of the batteries using different gel electrolytes are much lower than that of the battery using #33, the capacity retentions will be meaningless. Capacity is the most basic element of a battery. Under the premise of ensuring the capacity, the higher the capacity retention is, the better the cyclability is. Owing to the manganese dissolution, water evaporation, water decomposition, hydrogen evolution, and Zn corrosion … the capacity fading is observed on all batteries [39–41]. The initial discharge capacities at 4 C of batteries using the #33, 5% FS, 5% QAL/FS-1, and 5% QAL/FS-2 respectively, are nearly the same. Meanwhile, the coulombic

efficiencies at 4 C of all batteries for up to 1000 cycles are closed to 100%. Hence, it is very meaningful to evaluate the capacity retention of all batteries under this condition. The results are presented in Fig. 4b. After 1000 cycles, the capacity retentions of batteries using the #33, 5% FS, 5% QAL/FS-1, and 5% QAL/FS-2 are approximately 65.6%, 69.2%, 71.4% and 70.3%, respectively. Obviously, the capacity retention of battery using the 5% FS is higher than that of battery using the #33, which is advantageous of the gelled battery. After FS is coated with QAL, this advantage of FS is further improved, as evidenced by the slightly higher capacity retention of battery using 5% QAL/FS-1 and 5% QAL/FS-2 than that of battery using the 5% FS. In particular, the battery using 5% QAL/FS-1 presents the best cyclability, which means the better appropriate coating amount of QAL on FS for improving the cycle life of battery is 5 wt%.

In an effort of mimicking the industrial battery setting, we fabricated a bespoke cell which is larger than the coin cell and the cathode loading is 5.5 times higher than that in coin cells. This mean the cathode loading is about 33 mg $LiMn_2O_4$ per battery. In this large cell, the anode is pressed firmly and equally on the cathode (separated by the electrolyte-containing separator) and the system is hold firmly via support of two flat metal plates supporting the current collectors. The reference and the gelled batteries were tested by the same program used for coin cell, and the results are outstanding. We normally expect worse performance when increasing the cathode loading & size due to the limited Li^+ diffusion kinetics. However, the performance of the bespoke reference battery is slightly better than that of the coin cell (68% in large

cell vs. 65.6% capacity retention in coin cell). All cycling data exhibit less fluctuation thank to the firm support of the two holding plates, which always keeps the electrodes at parallel positions. This kind of support is not available in other kind of cells. The gelled batteries give 80–82% retention after 1000 cycles and this is about 14% higher than that of the reference battery. However, it is found that the enhancement in cyclability of gelled large battery is higher than that of aqueous large battery. This can be explained as follows. Our previous work has found that the water retention ability of ReHAB is poor, leading to pH and concentration change in the electrolyte which results in rapidly declining of the battery capacity [12]. The FS based gel electrolyte possesses much better water retention ability than the aqueous electrolyte [12]. In coin cell, the advantage of gel electrolyte in water retention is not able to be fully revealed because the amount of electrolyte is too limited (only three drops). In large battery, the amount of electrolyte is up to several milliliter so that the advantage of gel electrolyte in water retention can play its role. Thus, the gel electrolyte maximize their positive effects (e.g. lower corrosion, lower dendrite formation, higher preservation of water inventory …) in large battery compared with coin cell. All of these contribute to higher performance of gelled large batteries. This gives us hope when testing the battery at pilot scale (6-10 Ah capacity).

3.4 Potential static impedance spectroscopy (PEIS)

Potential static impedance spectroscopy (PEIS) results of batteries and half cells using different electrolytes are presented in Fig. S5a and S5b (Supporting

information). The Ohmic resistances of all batteries are almost the same except the battery using 5% FS, whose resistance is slightly higher than the other batteries. The half cell shows reversed results, which means that a large portion of the Ohmic impedance of the full cell might be allocated to the electrolyte - anode interface. The semicircle at high frequency of all batteries are nearly the same except the battery using 5% QAL/FS-2, the semicircle of which is slightly bigger than the other batteries. This suggests that the charge transfer resistance of the battery using 5% QAL/FS-2 is slightly higher than that of the other batteries. It may be due to that too much QAL will increase the viscosity of the gel electrolyte, resulting in slightly lower diffusion rate of Li^+ from the electrolytes through the interface between the electrolyte and the cathode to the inside of the cathode. The slopes at the low frequency range of all batteries are nearly the same, which suggests that the diffusion rates of Li^+ in the cathode lattice of all batteries are almost the same. This is supported by the results of half cells. The Ohmic impedance of the 5%QAL/FS-1 and the 5%QAL/FS-2 increases slightly, the charge transferred resistance also increases slightly while the calculated Li^+ diffusion data are not much different, except that on the 5%FS, which is slightly higher.

3.5 XRD and SEM analyses of the cathode and anode after cycling

After cycling, the batteries are de-assembled and the electrodes are collected, washed by deionized water and studied by XRD and SEM. The XRD and SEM of post-battery-run cathodes are presented in Fig. 5. The XRD shows that both carbon

KS-6 conductive additive and the $LiMn_2O_4$ retain their crystallinity. This is an indirect evidence that shows the oxygen revolution on the cathode and the mangansese dissolution are successfully mitigated because these side reactions would lead to amorphization of the crystalline KS-6 and $LiMn_2O_4$ materials. From the SEM images, traces of the gel electrolytes are found on the surface when using lignin coated silica gel electrolytes, even after careful washing (image C1, C2 (Fig. S6, Supporting information), D1, D2 in Fig. S6 (Fig. S6, Supporting information)). The post-run cathode of the reference battery (image B1, B2 (Fig. S6, Supporting information)) is clean from any traces of electrolyte.

The XRD and SEM of post-battery-run anodes are presented in Fig. 6. The XRD patterns of post-battery-run anodes are representative for zinc, but intensities of peaks are different. This reflects different developments of the zinc anode vs. cycling. From crystallography perspective, the zinc surfaces containing (100) and (110) planes support vertical dendritic zinc growth while (002) surface supports basal or flat zinc deposit [42–44]. In gelled battery using silica as the only gelling agent, the intensity of the (100) is not diminished and the (002) is not improved vs. cycling [12]. However, the situation changes completely when the surface of silica is coated by a suitable quantity of QAL. The (002) surface becomes dominant on the anode of the gelled battery using 5% QAL/FS-1 gel while the (100) peak diminishes. This is a very clear evidence that the dendrite is totally suppressed, as confirmed by the SEM results (images G1 and G2 (Fig. S7, Supporting information)). The G1 and G2 (Fig. S7, Supporting information) are much flatter than the F1 and F2 (Fig. S7, Supporting

information), which represent the anode of post-run reference battery. This result is supported by the low corrosion current density and low absolute value of chronoamperometry current density, complemented by a uniform Zn deposition (Fig. 2b). When Zn is deposited on the working electrode from a electrolyte with very low corrosive and good ability to support uniform growth of Zn, the Zn deposits may be basal type [30,44]. In such cases, the zinc deposits prefer (002) crystallographic orientation. In current case, the 5% QAL/FS-1 electrolyte is the optimal one in this paper. It exhibits low corrosion current density and simultaneously support uniform growth of Zn when in contact with a Zn working electrode, thus, it is expected that the morphology of the Zn deposit from this electrolyte is basal type, associated with highest relative intensity of the (002) XRD peak. Other patterns contain (002) peak, too. But the relative intensities are lower because we scale all patterns using (101) peak. The QAL/FS-2 electrolyte offers even better corrosion inhibition, reflected by lower corrosion current density and a massive upside move of the equilibrium corrosion potential. However, on the XRD, the (002) XRD peak is not dominant and the capacity retention of the QAL/FS-2 is less than the QAL/FS-1. This seems contradicting but it is explainable by analysis of the XRD without scaling in details. The XRD pattern without scaling of post-battery run of the battery using this electrolyte is presented in Fig. S8 (Supporting information). On this XRD, we clearly see the formation of ZnO and $Zn(OH)_2$ on the Zn surface even though Zn is still the dominant phase. This means too much lignin causes surface passivation. Its SEM (Fig.6 (H1)) shows that the surface is charged up when measurement took place and

this is due to the formation of ZnO and $Zn(OH)_2$ which are more insulating than the original Zn metal. Passivation clearly leads to less corrosion, however, it decreases the battery performance.

Conclusions

In summary, lignin was introduced into the ReHAB by preparing a novel gel electrolyte with the lignin coated FS for the first time. The advantages of 5% FS compared with the #33, for example, improvements on the performances of CA, float charge, rate, and cyclability, were further enhanced after the FS was coated by lignin. In particular, the disadvantage of 5% FS compared with the #33, for example, increase in the corrosion on Zn anode, was also improved after the FS was coated by lignin. Comparing the two available lignin coated FS based gel electrolytes, 5% QAL/FS-1 and 5% QAL/FS-2, the battery using 5% QAL/FS-1 showed slightly better rate and cycling performance and slightly lower charge transfer resistance, while the battery using 5% QAL/FS-2 presented much better ability to inhibit the corrosion on Zn and slightly better float charge performance. The capacity retention of large battery using 5% QAL/FS-1 is 82% after 1000 cycles at 4 C while this is 80% for the battery using 5% QAL/FS-2. This work provides new approach to develop green gel electrolytes for batteries and promotes the progress in research of high value-added application of green and sustainable lignin resource.

Acknowledgements

This research is financially supported by the National Natural Science Foundation of China (No. 21436004, 21576106), Natural Science Foundation of Guangdong Province (2017A030308012), Positec Canada Ltd., Chinese Scholarship Council (CSC), Mitacs (IT06145).

Appendix A. Supplementary Material

Supplementary data associated with this article can be found in the online version at …

References

[1] Y.G. Wang, J. Yi, Y.Y. Xia, Recent progress in aqueous lithium-ion batteries, Adv. Energy Mater. 2 (2012) 830–840.

[2] M. Pasta, C.D. Wessells, R.A. Huggins, Y. Cui, A high–rate and long cycle life aqueous electrolyte battery for grid–scale energy storage, Nat. Commun. 3 (2012) 1149.

[3] W. Tang, Y.S. Zhu, Y.Y. Hou, L.L. Liu, Y.P. Wu, K.P. Loh, H.P. Zhang, K. Zhu, Aqueous rechargeable lithium batteries as an energy storage system of superfast charging, Energy Environ. Sci. 6 (2013) 2093–2104.

[4] H. Kim, J. Hong, K.-Y. Park, H. Kim, S.-W. Kim, K. Kang, Aqueous rechargeable Li and Na ion batteries, Chem. Rev. 114 (2014) 11788–11827.

[5] N. Alias, A.A. Mohamad, Advances of aqueous rechargeable lithium-ion battery: a review, J. Power Sources 27 (2015) 237–251.

[6] J. Yan, J. Wang, H. Liu, Z. Bakenov, D. Gosselink, P. Chen, Rechargeable hybrid aqueous batteries, J. Power Sources 2 (2012) 222–226.

[7] Y. Wang, W.H. Zhong, Development of electrolytes towards achieving safe and high-performance energy-storage devices: a review, ChemElectroChem 2 (2015) 22–36.

[8] H. Zhang, C.M. Li, M. Piszcz, E. Coya, T. Rojo, L.M. Rodriguez-Martinez, M. Armand, Z.B. Zhou, Single lithium-ion conducting solid polymer electrolytes: advances and perspectives, Chem. Soc. Rev. 46 (2017) 797–815.

[9] A. Manthiram, X.W. Yu, S.F. Wang, Lithium battery chemistries enabled by solid-state electrolytes, Nat. Rev. Mater. 2 (2017) 16103.

[10] D.W.H. Lambert, P.H.J. Greenwood, M.C. Reed, Advances in gelled-electrolyte technology for valve-regulated lead-acid batteries, J. Power Sources 107 (2002) 173–179.

[11] A.A. Mohamad, Zn/gelled 6 M KOH/O_2 zinc–air battery, J. Power Sources 159 (2006) 752–757.

[12] C.Y. Lu, T.K.A. Hoang, T.N.L. Doan, H.B. Zhao, R. Pan, L. Yang, W.S. Guan, P. Chen, Rechargeable hybrid aqueous batteries using silica nanoparticle doped aqueous electrolytes, Appl. Energy 170 (2016) 58–64.

[13] T.K.A. Hoang, M. Acton, H.T.H. Chen, Y. Huang, T.N.L. Doan, P. Chen, Sustainable gel electrolyte containing Pb^{2+} as corrosion inhibitor and dendrite suppressor for the zinc anode in the rechargeable hybrid aqueous battery, Mater. Today Energy 4 (2017) 34–40.

[14] T.K.A. Hoang, T.N.L. Doan, J.H. Cho, J.Y.J. Su, C. Lee, C.Y. Lu, P. Chen, Sustainable gel electrolyte containing pyrazole as corrosion inhibitor and dendrite suppressor for aqueous Zn/$LiMn_2O_4$ battery, ChemSusChem 10 (2017) 2816–2822.

[15] S. Spange, E. Vilsmeier, Y. Zimmermann, Probing the surface polarity of various silicas and other moderately strong solid acids by means of different genuine solvatochromic dyes, J. Phys. Chem. B 104 (2000) 6417–6428.

[16] S.-H. Wu, C.-Y. Mou, H.-P. Lin, Synthesis of mesoporous silica nanoparticles, Chem. Soc. Rev. 42 (2013) 3862–3875.

[17] Y.Y. Ge, D. Xiao, Z.L. Li, X.M. Cui, Dithiocarbamate functionalized lignin for efficient removal of metallic ions and the usage of the metal-loaded bio-sorbents as potential free radical scavengers, J. Mater. Chem. A 2 (2014) 2136–2145.

[18] S. Laurichesse, L. Avérous, Chemical modification of lignins: towards biobased polymers, Prog. Polym. Sci. 39 (2014) 1266–1290.

[19] Y. Qian, Y.H. Deng, X.Q. Qiu, H. Li, D.J. Yang, Formation of uniform colloidal spheres from lignin, a renewable resource recovered from pulping spent liquor, Green Chem. 16 (2014) 2156–2163.

[20] Y. Qian, X.Q. Qiu, S.P. Zhu, Lignin: a nature-inspired sun blocker for broad-spectrum sunscreens, Green Chem. 17 (2015) 320–324.

[21] M. Lievonen, J.J. Valle-Delgado, M.-L. Mattinen, E.-L. Hult, K. Lintinen, M.A. Kostiainen, A. Paananen, G.R. Szilvay, H. Setälä, M. Österberg, A simple process for lignin nanoparticle preparation, Green Chem. 18 (2016) 1416–1422.

[22] D. Kai, M.J. Tan, P.L. Chee, Y.K. Chua, Y.L. Yap, X.J. Loh. Towards lignin-based functional materials in a sustainable world, Green Chem. 18 (2016) 1175–1200.

[23] T. Aro, P. Fatehi, Production and application of lignosulfonates and sulfonated lignin, ChemSusChem 10 (2017) 1861–1877.

[24] Y.N. Qu, Y.M. Tian, B. Zou, J. Zhang, Y.H. Zheng, L.L. Wang, Y. Li, C.G. Rong, Z.C. Wang, A novel mesoporous lignin/silica hybrid from rice husk produced by a sol-gel method, Bioresource Technol. 101 (2010) 8402–8405.

[25] X.J. Zhang, Z.H. Zhao, G.J. Ran, Y. Liu, S. Liu, B. Zhou, Z.C. Wang, Synthesis of lignin-modified silica nanoparticles from black liquor of rice straw pulping, Powder Technol. 246 (2013) 664–668.

[26] W.L. Xiong, D.J. Yang, R.S. Zhong, Y. Li, H.F. Zhou, X.Q. Qiu, Preparation of lignin-based silica composite submicron particles from alkali lignin and sodium silicate in aqueous solution using a direct precipitation method, Ind. Crops Prod. 2015;74:285-292.

[27] W.L. Xiong, X.Q. Qiu, D.J. Yang, R.S. Zhong, Y. Qian, Y.Y. Li, H. Wang, A simple one-pot method to prepare UV-absorbent lignin/silica hybrids based on alkali lignin from pulping black liquor and sodium metasilicate, Chem. Eng. J. 326 (2017) 803-810.

[28] H.J. Walls, J. Zhou, J.A. Yerian, P.S. Fedkiw, S.A. Khan, M.K. Stowe, G.L. Baker, Fumed silica-based composite polymer electrolytes: synthesis, rheology, and electrochemistry, J. Power Sources 89 (2000) 156–62.

[29] J.P. Sharma, S.S. Sekhon. Nanodispersed polymer gel electrolytes: conductivity

modification with the addition of PMMA and fumed silica, Solid State Ionics 178 (2007) 439–45

[30] K.E.K. Sun, T.K.A. Hoang, T.N.L. Doan, Y. Yu, X. Zhu, Y. Tian, P. Chen, Suppression of dendrite formation and corrosion on zinc anode of secondary aqueous batteries, ACS Appl. Mater. Interfaces 9 (2017) 9681-9687.

[31] G.G. Kumar, S. Sampath, Electrochemical characterization of poly(vinylidenefluoride)-zinc triflate gel polymer electrolyte and its application in solid-state zinc batteries, Solid State Ionics 160 (2003) 289-300.

[32] A.J. Allmand, H.C. Cocks, The polarization of zinc electrodes in neutral and acid solutions of zinc salts by direct and alternating currents. Part 1, Proc. R. Soc. Lond. A 112 (1926) 259-279.

[33] J.W. Diggle, A.R. Despic, J.O′M. Bockris, The mechanism of the dendritic electrocrystallization of zinc, J. Electrochem. Soc. 116 (1969) 1503–1514.

[34] J.J. Niu, B.E. Conway, W.G. Pell, Comparative studies of self-discharge by potential decay and float-current measurements at C double-layer capacitor and battery electrodes, J. Power Sources 135 (2004) 332-343.

[35] K.R. Bullock, Carbon reactions and effects on valve-regulated lead-acid (VRLA) battery cycle life in high-rate, partial state-of-charge cycling, J. Power Sources 195 (2010) 4513-4519.

[36] R. Dufo-López, J.M. Lujano-Rojas, J.L. Bernal-Agustín, Comparison of different lead-acid battery lifetime prediction models for use in simulation of stand-alone photovoltaic systems, Appl. Energy 115 (2014) 242-253.

[37] H.B. Zhao, C.J. Hu, H.W. Cheng, J.H. Fang, Y.P. Xie, W.Y. Fang, T.N.L. Doan, T.K.A. Hoang, J.Q. Xu, P. Chen, Novel rechargeable $M_3V_2(PO_4)_3$//Zinc (M = Li, Na) hybrid aqueous batteries with excellent cycling performance, Sci. Rep. 6 (2016) 25809.

[38] Z. Bakenov, I. Taniguchi, Electrochemical performance of nanostructured $LiM_xMn_{2-x}O_4$ (M=Co and Al) powders at high charge–discharge operations, Solid State Ionics 176 (2005) 1027-1034.

[39] G.J. Xu, Z.H. Liu, C.J. Zhang, G.L. Cui, L.Q. Chen, Strategies for improving the cyclability and thermo-stability of $LiMn_2O_4$-based batteries at elevated temperatures, J. Mater. Chem. A 3 (2015) 4092-4123.

[40] A. Konarov, D. Gosselink, Y.G. Zhang, Y. Tian, D. Askhatova, P. Chen, Self-Discharge of rechargeable hybrid aqueous battery, Ecs. Electrochem. Lett. 4 (2015) A151-A154.

[41] T.K.A. Hoang, T.N.L. Doan, K.E.K. Sun, P. Chen, Corrosion chemistry and protection of zinc & zinc alloys by polymer-containing materials for potential use in rechargeable aqueous batteries, RSC Adv. 5 (2015) 41677-41691.

[42] Y. Sawada, Transition of growth form from dendrite to aggregate, Physica 140A (1986) 134-141.

[43] D.J. Mackinnon, J.M. Brannen, P.L. Fenn, Characterization of impurity effects in zinc electrowinning from industrial acid sulphate electrolyte, J. Appl. Electrochem. 17 (1987) 1129-1143.

[44] K.E.K. Sun, T.K.A. Hoang, T.N.L. Doan, Y. Yu, P. Chen, Highly sustainable zinc

anodes for a rechargeable hybrid aqueous battery, Chem. Eur. J. 23 (2017). DOI: 10.1002/chem.201704440

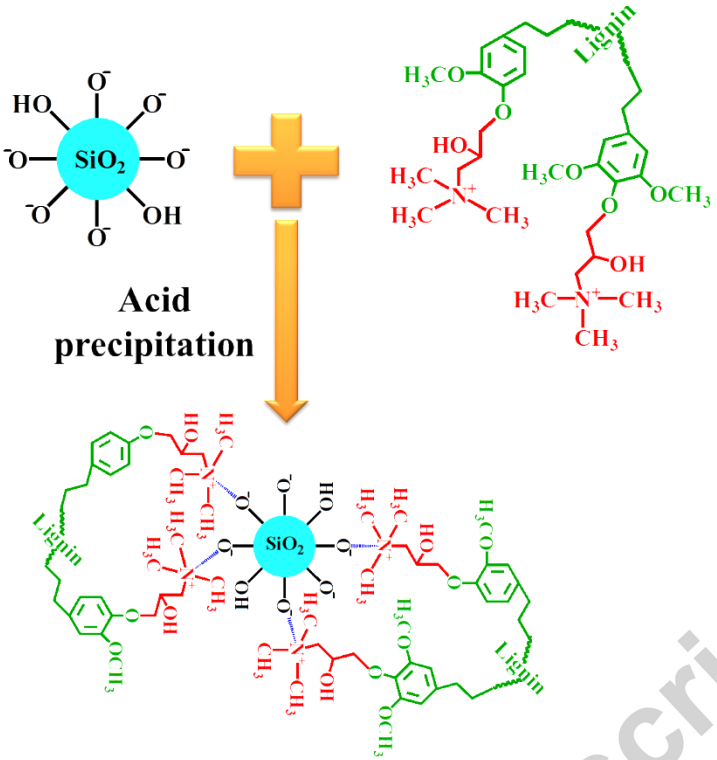

Scheme 1. Structure of FS, QAL, and the prepared QAL/FS composite.

Fig. 1. Linear polarization curves of zinc upon contact with different electrolytes.

Fig. 2. (a) Chronoamperometry (CA) current responses on zinc upon contact with different electrolytes; (b) SEM images of the post–run working electrodes of the CA studies in different electrolytes.

Fig. 3. (a) Float charge current of the batteries with different electrolytes after maintaining at 2.1 V by CV charging for 24 hours; (b) Rate capability of batteries using different electrolytes.

Fig. 4. (a) Cyclability and coulombic efficiency of the coin cells at 4 C rate; (b) Capacity retention of the coin cells at 4 C rate; (c) Cyclability of the large batteries at 4 C rate.

Fig. 5. (a) XRD patterns of the $LiMn_2O_4$ (LMO) cathodes from different large batteries after 1000 cycles at 4 C rate; (b) SEM images of the corresponding LMO cathodes: (A1) initial LMO cathode, (B1) LMO cathode (#33), (C1) LMO cathode (5% QAL/FS–1), (D1) LMO cathode (5% QAL/FS–2).

Fig. 6. (a) XRD patterns of the zinc anodes from different large batteries after 1000 cycles at 4 C rate; (b) SEM images of the corresponding zinc anodes: (E1) Pure zinc, (F1) zinc anode (#33), (G1) zinc anode (5% QAL/FS–1), (H1) zinc anode (5% QAL/FS–2).

Fig. 1

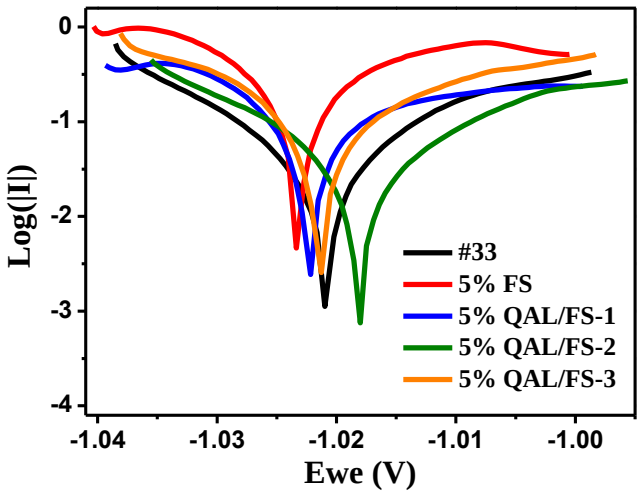

Fig. 2

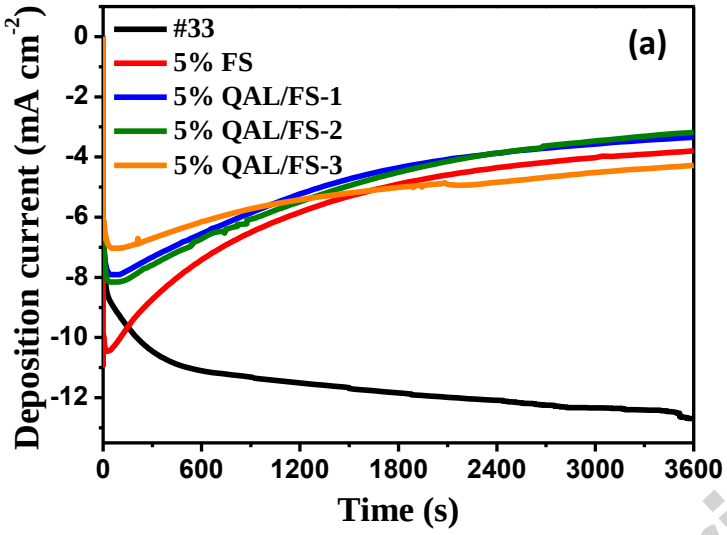

(b)

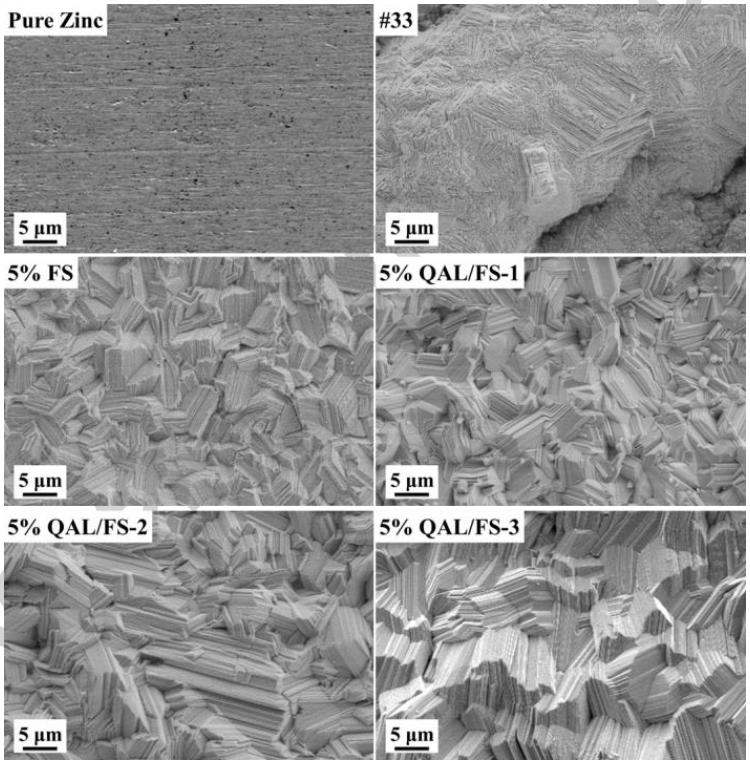

Fig. 3

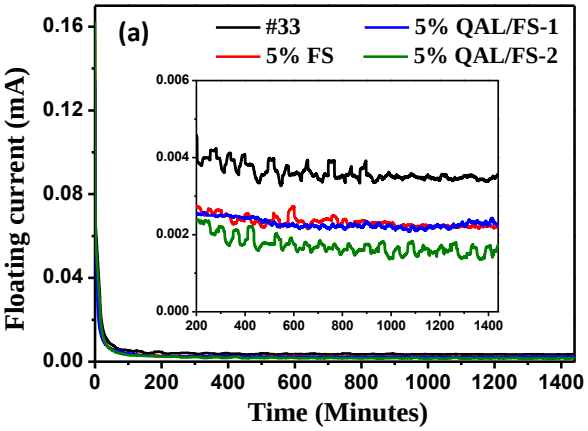

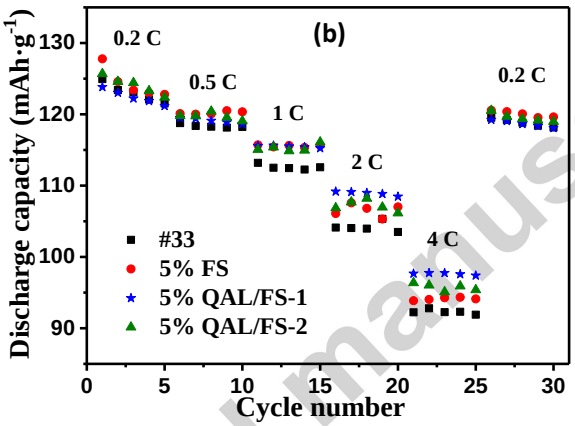

Fig. 4

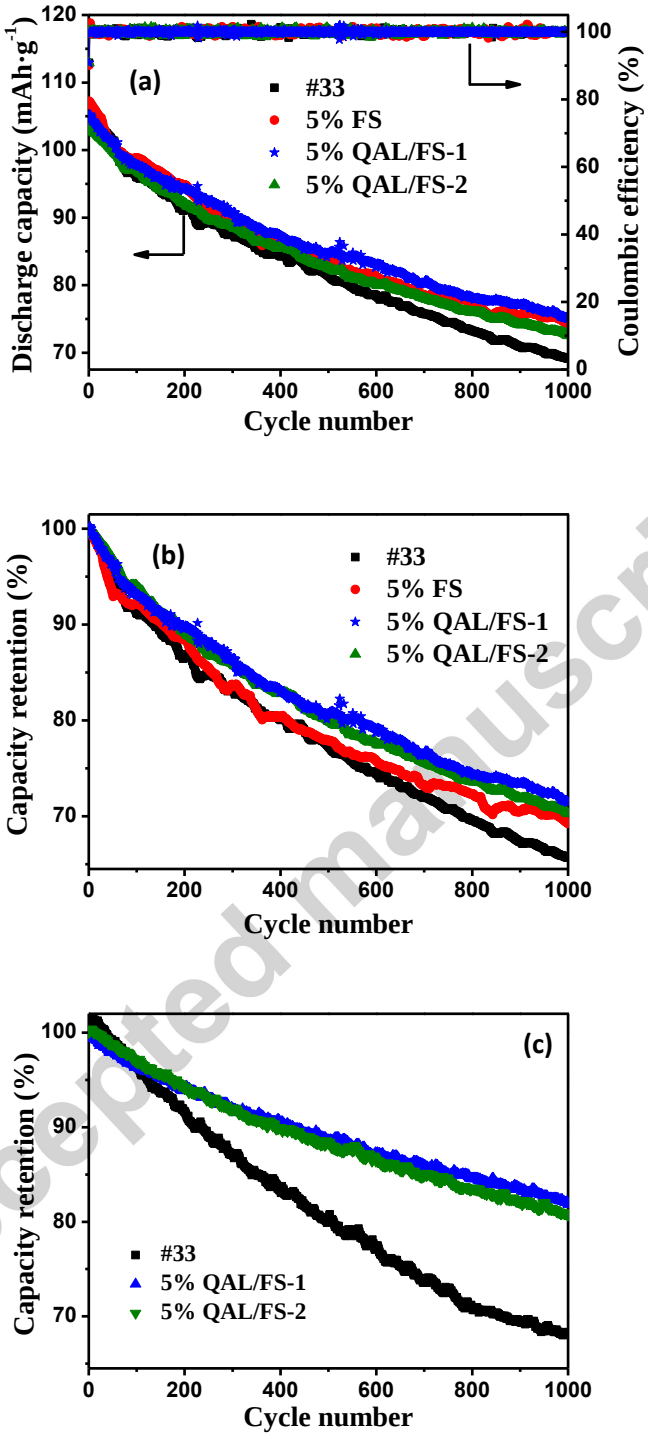

Fig. 5

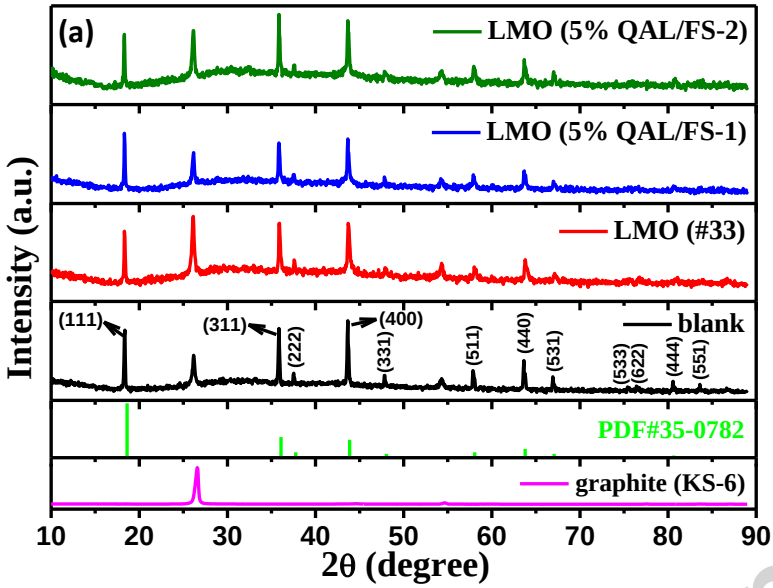

(b)

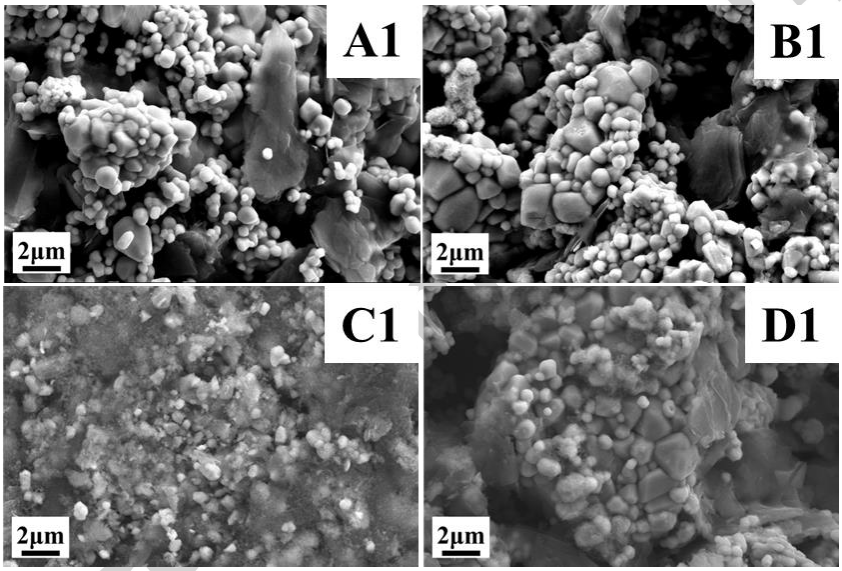

Fig. 6